ELSEVIER

Polymer crystallization from the metastable melt: The formation mechanism of spherulites

Masayuki Imai [1], Keisuke Kaji *

Institute for Chemical Research, Kyoto University, Gokasho, Uji, Kyoto-fu 611-0011, Japan

Abstract

One of the most popular crystalline morphologies is a spherulite. An evidence is reported that the spherulite is crystallized through a dense packing state of small particles appearing in a droplet, which is caused by the primary phase separation of the melt in the metastable region of a phase diagram proposed by Olmsted et al. [Olmsted PD, Poon WCK, McLeish TCB, Terrill NJ, Ryan AJ. Phys Rev Lett 1998; 81: 373]. According to this phase diagram, the crystallization from the metastable state causes the nucleation and growth (N & G) of nematic domains, here named droplets, in the isotropic matrix. As a next step, the secondary phase separation of spinodal decomposition (SD) type into smectic and amorphous domains occurs inside the droplet where entanglements are excluded from the smectic to the amorphous domain; then such an SD structure turns into a densely packing structure of many small particles owing to surface tension. At this final stage of the induction period a long period peak of small-angle X-ray scattering (SAXS), so-called SAXS before WAXS, appears, which may be due to the average distance between these small particles. Furthermore, it is considered that crystalline lamellae are formed by radial and azimuthal fusion of these small particles inside the droplet, resulting in a spherulite. Such a type of crystallization occurs most commonly when flexible polymers are crystallized under the usual conditions. This tentative concept of spherulitic growth, which is completely different from a theory by Keith and Padden [Keith HD, Padden FJ. J Appl Phys 1963; 34: 2409], would give a new insight into problems of spherulites.
© 2006 Elsevier Ltd. All rights reserved.

Keywords: Spherulites; Nucleation and growth (N & G); Spinodal decomposition (SD)

1. Introduction

Polymer spherulites were first discovered in the crystallization of cellulose triacetate solution with a polarized microscope by Hess [1]. Later, Bunn and Alcock [2] found spherulites of polyethylene in a thin film by observing the Maltese cross rotating on the spherulite in the polarized microscope when crossed polarizers were rotated, meaning that crystal entities orient radially, and they presumed from the measurements of optical refractive indices that the molecular axis is perpendicular to the radius of the spherulite. This molecular orientation was directly confirmed from the measurements of micro-beam X-ray diffraction by Keller [3].

Thereafter, many papers about the spherulites crystallized from the melt appeared as reviewed, for examples by Wunderlich [4] and Bassett [5,6]. The chain conformations in the crystalline morphologies, which were mainly revealed by small-angle, intermediate-angle and wide-angle neutron scattering techniques with a labelling method, were reviewed by Kaji [7].

As regards the mechanism for spherulitic growth in the melt, Keith and Padden [8] proposed an elaborate model on the basis of the assumptions of impurity segregation and cellulation (or fibrillation) even for homopolymers. They considered that a spherulite consists of a radiating array of crystalline fibres with non-crystallographic small-angle branching to fill the spherical space, and the reason for the fibre formation was explained as follows. The fibres are produced by the effect of impurities such as low molecular weight components and stereo-irregular components of the polymer, which are segregated and rejected preferentially from growing crystals. When the impurity-rich layer is constitutionally supercooled due to its lower equilibrium liquidus temperature, it tends to crystallize if the additional latent heat is transported away. Small projections at the

* Corresponding author. Present address: 1-1-5-304, Uchihirano-machi, Chuo-ku, Osaka 540-0037, Japan.
  E-mail addresses: imai@phys.ocha.ac.jp (M. Imai), kajiksk@ybb.ne.jp (K. Kaji).
[1] Present address: Department of Physics, Faculty of Science, Ochanomizu University, Otsuka, Bunkyo-ku, Tokyo 112-0012, Japan.

interface provide such conditions since the latent heat is transported away from the cellular interface and hence the system settles down in a cellular growth regime. Furthermore, at the tips of fibres exposed to virgin melt the surface nucleation rates are relatively fast but on lateral surfaces exposed only to residual interfibrillar melt containing segregated impurities they are relatively slow. Such an impurity-rich layer formed at the interface was estimated to have a thickness $\delta = D/G$, where D is the diffusion coefficient of impurity in the melt and G is the advancing velocity of a growing crystal face, which is nearly equal to the average cell diameter. They also suggested that the singularities such as screw dislocations or local temperature gradients act as effective nuclei for noncrystallographic small-angle branching of the cells (fibres). When the size of a growing crystal is commensurate with δ, it grows persistently. If much larger than δ, it breaks up into a number of smaller cells while if much smaller, it is swallowed up by other cells of more propitious size.

Bassett and coworkers thereafter examined this theory extensively by observing spherulitic growth and possible cellulation, finding that in the case of homopolymers such as polyethylene (PE) and polypropylene (PP) fibrils is not observed but wide lamellae are always produced. Hence, the morphological instability is not the cause of spherulitic growth in polymers; the impurity segregation, even if it slightly exists, is a secondary effect [9–14]. On the other hand, they actually observed using homologous copolymers such as various kinds of branched polyethylenes that when a great amount of impurity is included in the parent polymers, the cellulation occurs inside the spherulite; this new finding led them to a unified context for spherulitic growth in polymers [10,11]. From the observations with the transmission electron microscope that the dominant lamellae branch repeatedly often at giant screw dislocations, they proposed a different concept for the usual spherulitic growth of polymers [6] where the lamellae inside the spherulite were assumed to diverge substantially driving from pressure of uncrystallized molecular cilia [15–17].

Nevertheless, it seems that we have not yet well understood under which conditions and how the spherulites are produced. In this paper a tentative model of spherulitic growth from the polymer melt will be proposed, based on our new finding that at the initial stage of crystallization many densely packed small particles are observed inside the spherulite. We have recently reviewed our concept on polymer crystallization, especially in the very early stages prior to crystal nucleation [18], which is based on a theoretical phase diagram of polymer melt as functions of normalized density of the polymer melt and temperature proposed by Olmsted and coworkers [19] and our experimental observations [20–32]. In regards to the early stages of polymer crystallization controversial discussions have been made by several research groups such as Strobl [33], Ryan and coworkers [34–36], Hsiao and coworkers [37,38], Muthukumar and coworkers [39,40] and others, which were reviewed critically in our recent review article [18] as well.

In the following our model for the early stages of polymer crystallization [18] will be briefly explained for the readers' reference.

According to the Olmsted's phase diagram [19], a polymer liquid (melt) falls into a state, co-existence, metastable or unstable, with increasing the quenching depth ΔT, the difference between the equilibrium melting temperature of the polymer and a quenching (crystallization) temperature. In the co-existence state above the binodal temperature T_b, crystal nucleation occurs directly from the melt, producing probably single crystals in the melt matrix, though the rate of crystallization is extremely slow; in this case the crystal nucleation may obey a mechanism proposed by Boon, Challa, and van Krevelen [41,42]. Thus, the rate of nucleation is proportional to the product of transport factor and nucleation factor, the latter of which is a function of the Gibbs free energy of formation of a nucleus having a critical size, which is further a function of supercooling. On the other hand, the usual crystallization with a considerable rate always involves phase separation; the quench into below T_b causes phase separations. The most popular case for flexible polymers such as polyethylene (PE) and polypropylene (PP) is the quench into the metastable region between the binodal temperature T_b and the spinodal temperature T_s where optically anisotropic droplets of oriented (nematic) domains, probably having a molecular orientation perpendicular to the radius of the droplet, are first produced in the isotropic matrix by the primary phase separation of nucleation and growth (N & G) type. Furthermore, the quench into the unstable region below T_s causes a spinodal decomposition (SD) type phase separation into unoriented (isotropic) and oriented (nematic) phases. A drastic morphological change from N & G to SD pattern was observed by optical microscopy at $T_s = 213\ ^\circ\text{C}$ for poly(ethylene terephthalate) (PET) [30]. After these primary phase separations, the resulting nematic phase inside the droplet caused by N & G or in the oriented domain by SD undergoes the secondary phase separation of SD type again prior to crystal nucleation; it separates spinodally into a smectic phase and an amorphous phase. Then, the latter SD structure changes to a small particle packing structure due to the surface tension. During this process the molecular entanglements contained in the nematic phase should be excluded from the domains of smectic phase into the amorphous domains. Such small particles caused by the secondary phase separation of SD type eventually become densely packed, so that their average nearest-neighbour distance should provide a long period before crystal nucleation, which is so-called 'SAXS before WAXS'. Finally, the crystalline lamellae are formed by radial and azimuthal fusion of these small particles inside the droplet with the transformation from the smectic to crystalline structure where a sliding mechanism of molecular chains along the molecular axis would work as proposed by Flory [43], and the droplet transforms to the usual crystalline spherulite as a whole.

In this paper we will provide detailed evidences for PET using scanning electron microscopy (SEM), light scattering (LS), and small- and wide-angle X-ray scattering (SAXS and

WAXS, respectively) that a dense packing state of the small particles appear in the growing spherulite, and discuss the growing mechanism of spherulites.

2. Experimental

Samples of PET, supplied from Toyobo Co. Ltd, had a number-averaged molecular weight $M_n=25,000$ and a polydispersity $M_w/M_n=2.5$. The PET samples were prepared as follows: first thin films were made from ca. 1 wt% hexafluoroisopropanol solution on cover glass plates by a casting method and then melted at 290 °C for 2 min on a temperature-controlled hot-stage for optical microsopy and thereafter annealed at 220 °C for fixed times on the same hot-stage. After annealing the samples were quenched in ice–water to fix their structures.

Scanning electron microscope (SEM) observations were made using a Hitachi S-800 field emission type. The fixed-time annealed samples were immediately quenched in ice–water. The quenched samples were coated with Pt–Pd and then SEM observations were carried out at a low accelerated voltage of 5 kV for the sake of avoiding the sample damage. Observation of the internal structure of spherulites was performed using the samples fractured in liquid nitrogen. On the other hand, the time-resolved light scattering measurements during the annealing processes were carried out by heating the quenched sample on the temperature-controlled hot-stage at 220 °C. In these measurements we paid a special attention to the purity of the sample and optical parts to reduce the background scattering. A plane polarized He–Ne laser beam ($\lambda=633$ nm) was used, which was passed through a two-aperture system to eliminate parasitic scattering. The sample on the hot stage was irradiated by the beam and the scattered light intensity was recorded by a photometer system with a 38 photodiodes array [25]. The scattering measurements were carried out in a time slice of 100 ms under both Hv (cross polarized) and Vv (parallel polarized) optical geometries. In order to detect the weak intensity change exposure time was taken to be 2 s and the measurements were performed several times to check reproducibility.

Annealed samples were also investigated using SAXS and WAXS techniques. The SAXS measurements were performed on the 6 m point focusing SAXS camera at the High-Intensity X-Ray Laboratory of Kyoto University [44]. This camera utilizes Ni-filtered Cu Kα radiation from a 3.5 kW rotating-anode X-ray generator (RU-1000C3, Rigaku Denki Co. Ltd, Japan), Franks-type double-focusing point collimator, and two-dimensional position sensitive proportional counter. The scattering intensity after subtraction of the background was circularly averaged since the scattering patterns were azimuthally isotroic. The measurements were carried out for two Q ranges of 0.01–0.05 and 0.04–0.2 Å^{-1}. The observed scattering curves in these two Q ranges were superposed by vertical shift so that they would agree best with each other in the overlapped Q-range. The WAXS measurements were carried out using Ni-filtered Cu Kα X-ray generated from 4.0 kW Rigaku RAD-rA with a pinhole collimation system.

3. Results

3.1. Crystallization isotherm and macroscopic density

The glass transition and melting temperatures of the PET sample were 75 and 250 °C, respectively. Fig. 1 shows the crystallization isotherm $\phi(t)$ measured by a differential scanning calorimeter (DSC) and the observed densities as a function of crystallization time at 220 °C. The isotherm was calculated according to the following equation.

$$\phi(t) = \frac{\int_0^t (dH_\tau/d\tau)d\tau}{\int_0^\infty (dH_\tau/d\tau)d\tau} \tag{1}$$

where dH_t/dt is the rate of heat evolution. Both curves are similar and have a sigmoidal shape being typical of polymer crystallization behaviour. The crystallization isotherm begins to increase immediately after the temperature attained 220 °C and levels off at an equilibrium value after about 2 h of annealing time.

3.2. WAXS and SAXS

In order to know when crystallization starts, we measured WAXS at 220 °C as a function of crystallization time in a time
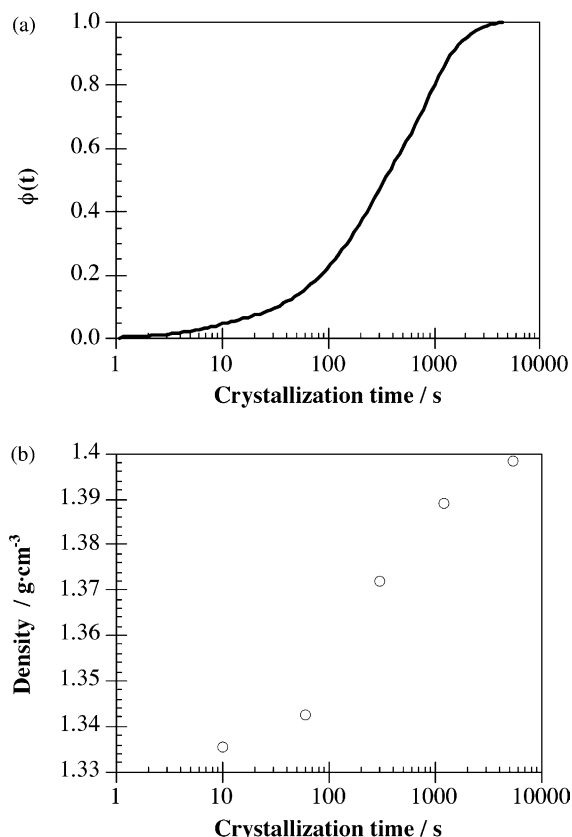

Fig. 1. Annealing time dependences of crystallization isotherm (a) and the macroscopic density (b) for PET. Annealing temperature: 220 °C.
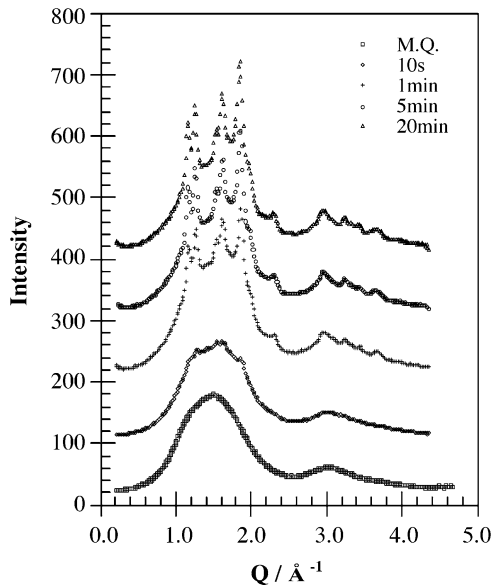
Fig. 2. Crystallization time dependence of the WAXS profile for PET at 220 °C.

3.3. Morphological observations

Morphological observations were carried out by optical microscopy, which are given in Fig. 4. Fig. 4a shows a polarized optical micrograph of typical spherulites in the growing process when the PET sample was annealed for 30 min at 220 °C, exhibiting the extinction rings and Maltese crosses, and Fig. 4b indicates a SEM photograph for the same spherulites. The latter photograph indicates that a spherulite is composed of fibrils radiating from the center with branching to fill the space; the average diameter of the fibrils is about 0.2–0.5 μm. We also observed the fracture surface of a spherulite to reveal the internal structure of the spherulite at the initial stage, which is shown in Fig. 5. Surprisingly, many closely packed small particles are seen on the fracture surface of the growing spherulite. The average diameter of these

range of 0–20 min. As seen from Fig. 2, the melt-quenched (M.Q.) sample shows only broad amorphous peaks but in 10 s weak diffraction peaks have already appeared, so that the induction period of crystallization in this case is less than 10 s. In the same time range we also measured SAXS and the results are shown in Fig. 3. The melt-quenched sample shows a broad central peak which may be due to the so-called Fischer's cluster with a few thousands Angstrom existing usually in the amorphous materials. In 10 s a broad peak emerges at around 0.04 Å^{-1} and increases in intensity with time. This peak may be assigned to the so-called long period because the crystallization has already occurred.
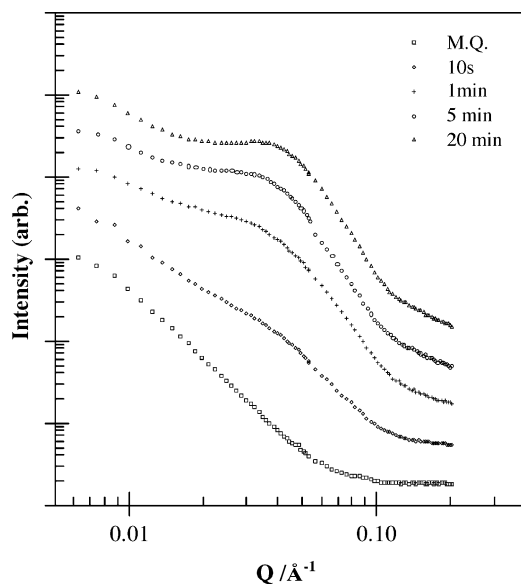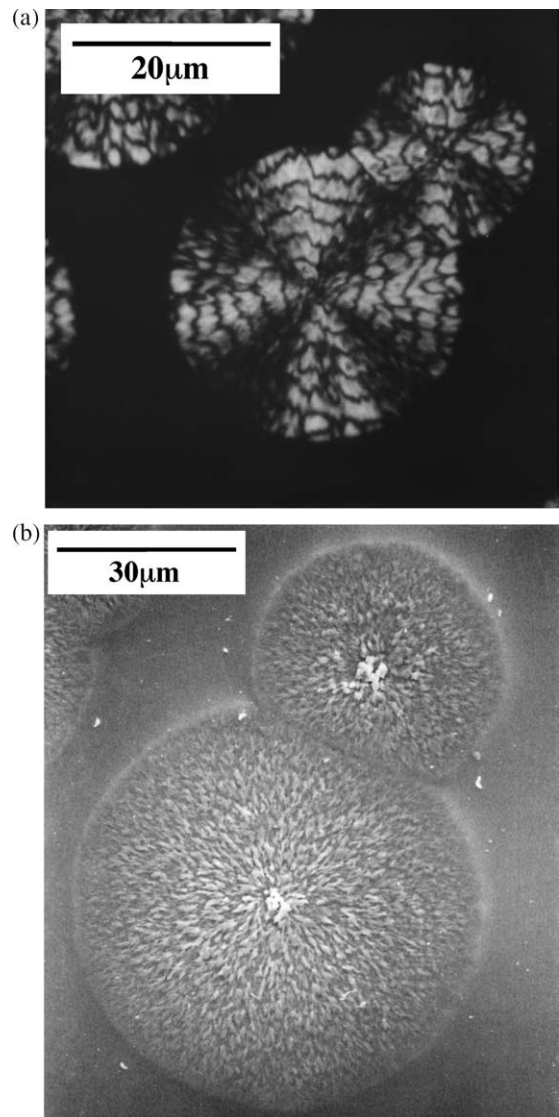

Fig. 4. Polarized optical micrograph (POM) (a) and scanning electron micrograph (SEM) (b) of spherulites in PET samples annealed for about 30 and 60 min, respectively, at 220 °C. The POM shows the extinction rings and Maltese crosses. Both the POM and the SEM indicate band structure.
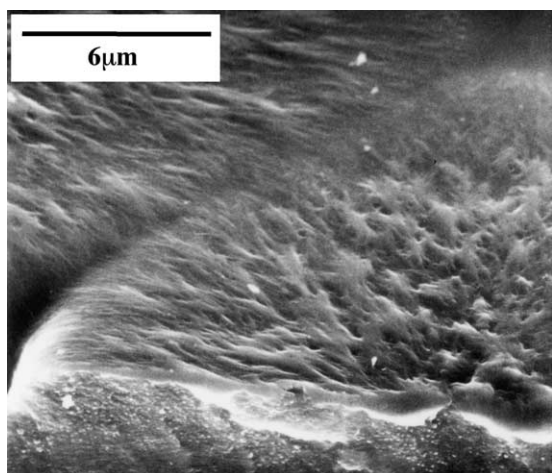

Fig. 3. Crystallization time dependence of the SAXS profile in logarithmic scales for PET at 220 °C.

Fig. 5. SEM photograph of a fractured spherulite in the PET sample annealed at 220 °C.

particles is about 0.2–0.3 μm, which corresponds to that of the fibrils observed on the surface of the growing spherulite. In what follows let us examine such a particle structure.

When do the small particles begin to appear during the crystallization process? First, we observed the morphological change of the fracture surface of a growing spherulite. Fig. 6 shows such results; the amorphous sample obtained by quenching from the molten state does not show the particle structure but smooth surface (see Fig. 6a). In 10 s after annealing at 220 °C small particles start to emerge though they are sparsely populated and their size is very small. At this early stage the crystallinity of the sample calculated from the density was about 3%, so that in 10 s the crystal nucleation has already started. However, it may be considered that at the instance of the particle formation the internal structure is smectic, which soon transforms to crystal nuclei because the crystallization rate is high at this temperature. The particle structure becomes clearer with annealing time, and the
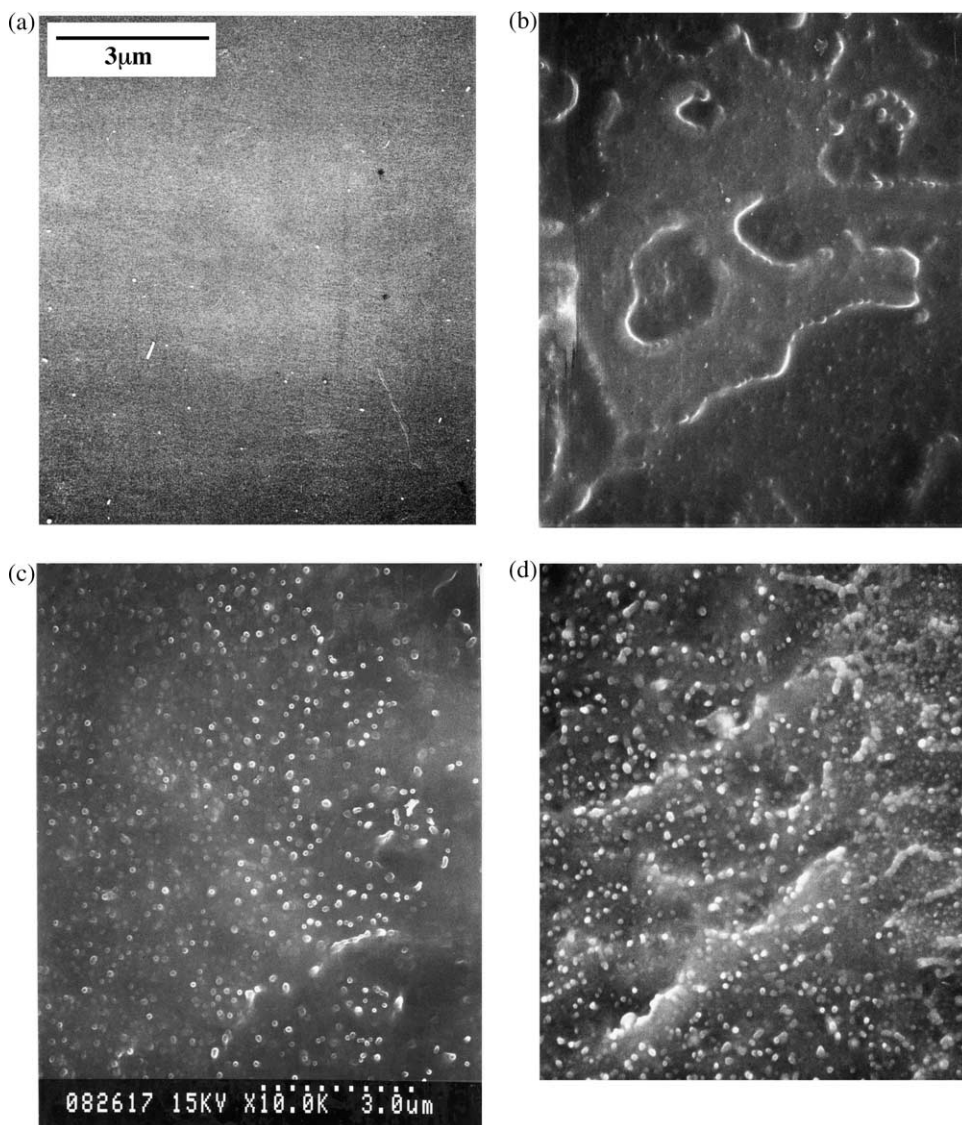

Fig. 6. Morphological change observed on the fractured surface of the PET samples as a function of crystallization time at 220 °C. (a) As melt quenched, (b) annealed for 10 s, (c) 5 min, and (d) 20 min.

average particle size slightly increases though it seems to level off. Before considering the role of this particle structure in the growth process of spherulites, we should first remove the question whether or not this structure is an artifact when the samples were prepared, for example, fractured for SEM observations. In order to take away this doubt we examined the particle structure in the following three points: (1) Is the particle structure observed on the spherulite surface as well? (2) Does the particle superstructure respond to deformation? (3) Can we in situ observe the particle structure during crystallization by means of a light scattering technique? Fig. 7 shows an evidence for the first point; as seen from such an enlarged SEM photograph of the spherulite surface, the small particles exist among branched fibrils. This means that the particle structure is common both in the surface region and inside the spherulite. However, the former particle structure is somewhat obscure. This may be because the fusion of the particles into the fibrils has proceeded more profoundly in the surface layer where the quenching effect is larger. For the second point, we examined the behaviour of the superstructure of the particles in a stretched PET film. If the particle structure is an artifact appearing when the sample was fractured, their superstructure should be independent of the stretching deformation while if it is real, the superstructure should be deformed by stretching. Fig. 8 shows the SEM photograph of the fracture surface of a PET film drawn by two times at 110 °C. As seen from this photograph, particles are aligned to the draw direction, keeping their outer spherical shape. Thus, the interparticle deformation was caused by stretching; in other words the particles moved relatively during the deformation. The above described results support that the particle structure is not an artifact but the real one, which is formed in an early stage of crystallization. The third point will be described in the following subsection 3.4.
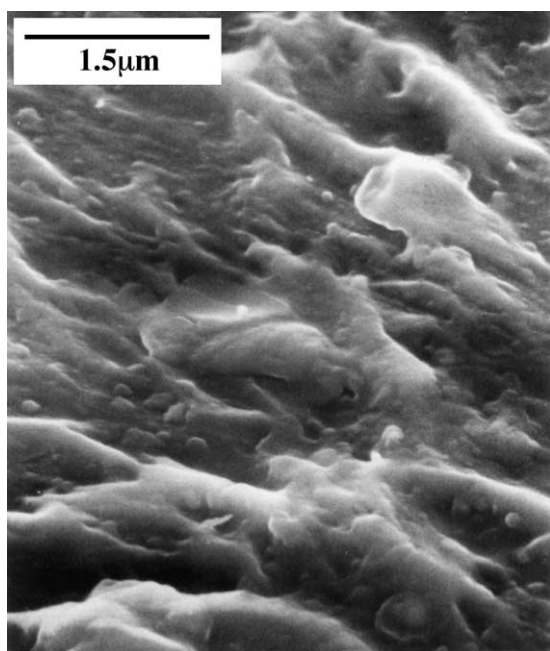

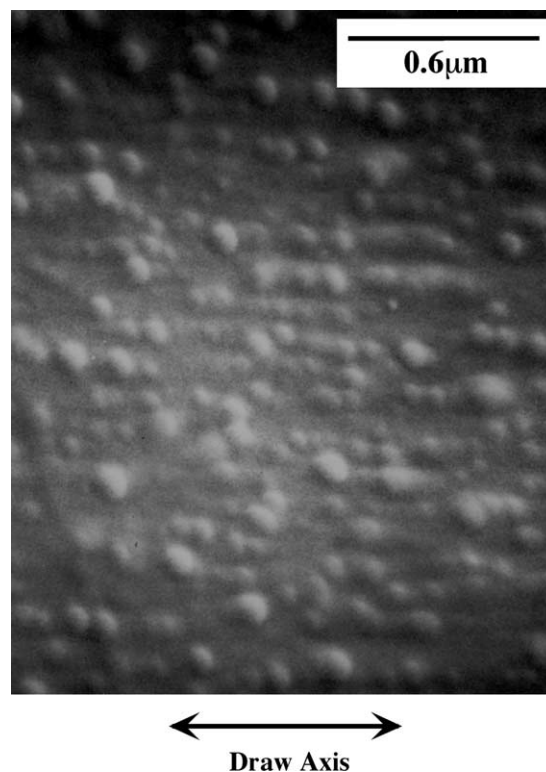Fig. 7. Enlarged SEM photograph of the spherulite surface of PET in Fig. 5.

Fig. 8. SEM photograph of fracture surface of a PET film drawn by two times at 110 °C.

3.4. In situ observations by light scattering

The time development of the crystallization processes can be investigated by the time-resolved light scattering measurements under the Hv and Vv geometries. The Hv scattering shows only the contribution from orientation fluctuations, while the Vv scattering shows contributions due to both density and orientation fluctuations.

First, the Hv scattering is explained. Fig. 9 shows Hv scattering profiles as a function of the crystallization time, which gives information about the superstructure of molecular orientation. As is seen from this figure, the scattering curves in the initial time until 50 s decrease monotonously with increasing Q as far as the observed range is concerned. However, they may be assumed to be almost constant in this Q range because the intensities at lower Q values can be considered the tail of scattering from the direct beam. After 70 s, a broad maximum appears at around $Q = 2.0 \ \mu m^{-1}$ with decreasing to $1.2 \ \mu m^{-1}$ in 350 s. This maximum can be assigned to the scattering from the optically anisotropic spheres of the droplets, i.e. the nuclei caused by the N & G mechanism in the primary phase separation from the metastable state, because the peak position decreases with crystallization time. According to Samuels [45], the Hv scattering from an optically anisotropic sphere with a radius R_0 gives a maximum intensity on a four leaves pattern at

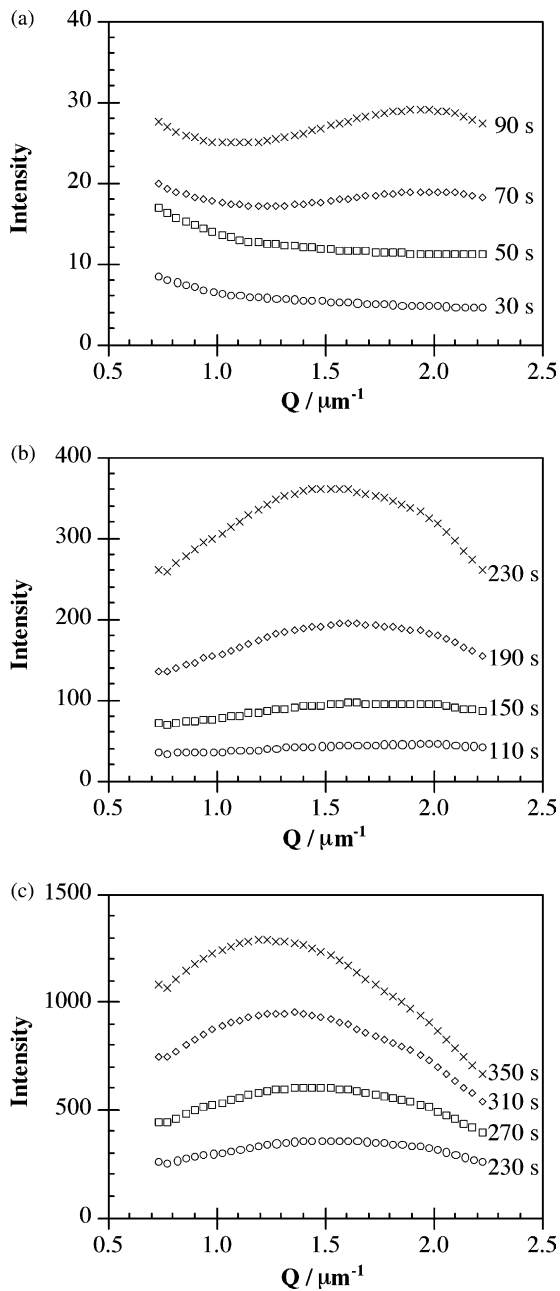$$Q_m = \frac{4.02}{R_0}. \tag{2}$$

(a)

(b)

(c)

Fig. 9. Hv light scattering profiles of PET as a function of crystallization time. (a) 30–90 s, (b) 110–230 s, and (c) 230–350 s. Crystallization temperature: 220 °C.
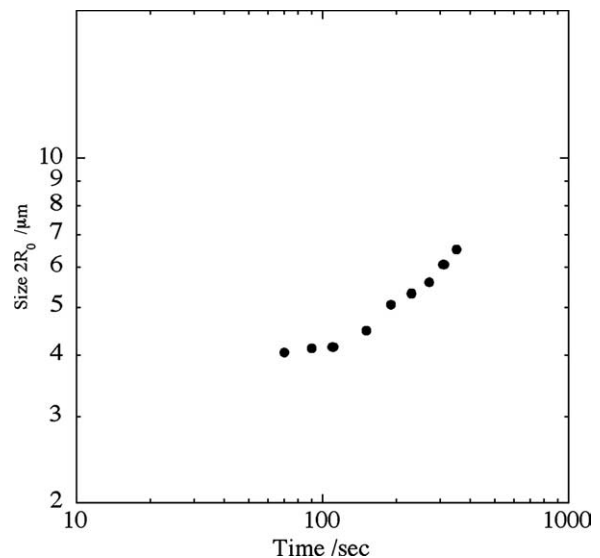

Fig. 10. Size of the droplets as a function of crystallization time, determined from the peak positions of Hv scattering using Eq. (2). $2R_0$ is the diameter of the droplet.

of Fig. 4(a) since the interspace of the periodic extinction rings hardly changes with time. As is well known, such extinction rings are caused by the twisting of crystalline lamellae [4]. Therefore, this corresponds to the stage after the fusion of the small particles into crystalline lamellae though it occurs partially on the surface of the droplet at this stage.

In the following the results of Vv scattering are described. Fig. 11 shows the time evolution of the Vv scattering profiles which were obtained by subtracting the intensity of the melt from those of annealed samples. These scattering curves decrease monotonously as Q increases within the observed Q range of 2–6 μm^{-1}. The scattering intensities at lower Q's, which are not the tail of the direct beam because the observed Q range is very high, increase rapidly between 20 and 30 s in crystallization time; this seems arise from the increase in size of the particles as seen from the SEM photographs in Fig. 6. The quantitative analysis for these scattering curves has been

Thus, the average size, $2R_0$, of the droplets can be estimated using this equation; the results are shown in Fig. 10. It changes from 4.0 to 6.7 μm for 70–350 s. If the growth rate of the droplet is assumed to be constant, these values will be reasonable judging from the polarized and SEM micrographs for the samples annealed for about 30 and 60 min, respectively, in Fig. 4. Then, the critical size of the nucleus in the N & G mechanism may exist because $2R_0$ levels off below 100s, which seems to be less than 4.0 μm. Furthermore, a shoulder observed at ca. 2.0 μm^{-1} after 190 s might be due to the interspace (ca. 3 μm) of the periodic extinction rings of the banded spherulite observed in the polarized optical micrograph
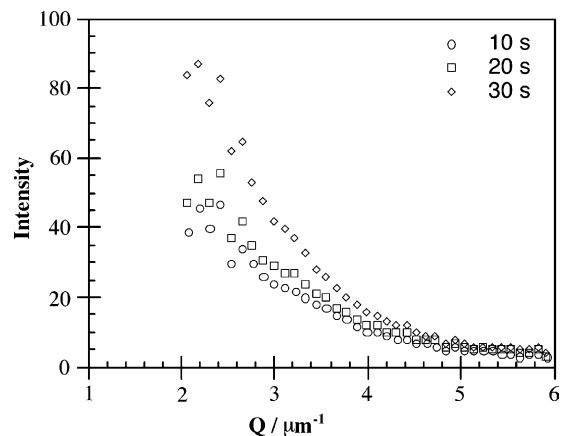

Fig. 11. Vv light scattering profiles of PET as a function of crystallization time in a time range of 0–30 s. Crystallization temperature: 220 °C.

made, based on a scattering theory developed for an inhomogeneous solid by Debye and Bueche [46]. According to this theory, the scattering function for inhomogeneous solids is given as

$$I(Q) = \frac{A}{(1 + a^2 Q^2)^2} \qquad (3)$$

where A is a constant, Q is the length of scattering vector ($Q = 4\pi\sin(\theta/\lambda)$) and a is a correlation length defined by the correlation function $\gamma(r)$:

$$\gamma(r) = \exp\left(\frac{-r}{a}\right). \qquad (4)$$

The correlation length a corresponds to the short-range fluctuation in the inhomogeneous system. In the present system it may correspond to the interparticle correlation distance or roughly to the average distance between the nearest-neighbour particles. Hence, we employ this technique to confirm the existence of the particle texture observed in the SEM photographs.

Using Eq. (3) let us estimate the correlation lengths for various crystallization times. Fig. 12 shows the plot of $I^{-1/2}$ against Q^2 for a sample annealed for 10 s as an example; a linear relationship is obtained in the observed Q range, providing a correlation length of about 0.4 μm from the slope and the intercept. All the estimated correlation lengths are plotted as a function of crystallization time in Fig. 13. As seen from this figure, the correlation length $a \cong 0.4$ μm hardly changes until 30 s. These values agree well with the nearest-neighbour interparticle distances as seen in the SEM photographs in Fig. 6(b) and (c). Thus, in the initial time until 30 s the particle size increases with time, but the nearest-neighbour interparticle distance is almost constant.

Judging from Fig. 6, the number density of the small particles at 20 min is so large that the interparticle interferences can be presumed. Actually, Herglotz [47] investigated a PET film heat-treated at 225 °C for 300 s using cabon K radiation, a long wavelength X-ray with $\lambda = 4.47$ nm, finding a diffraction peak corresponding to the Bragg spacing of about 0.14 μm,

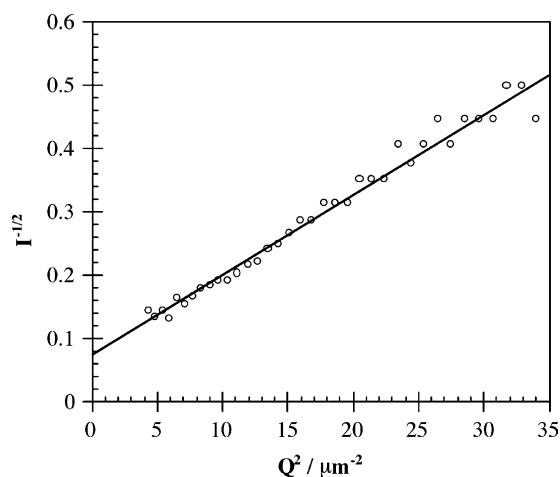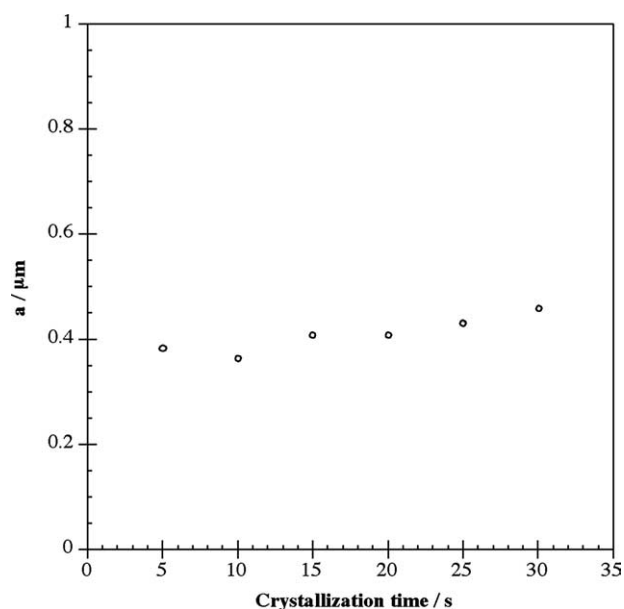Fig. 13. Crystallization time dependence of the correlation length a among the small particles in the PET sample. Crystallization temperature: 220 °C, and the time range: 0–30 s.

which is in the same order with the above correlation length and the interparticle distance at 20 min in Fig. 6.

Finally, the integrated intensities of the Hv and Vv scattering with time have been calculated. Koberstein et al. [48] showed that the orientation and density fluctuations can be expressed by the total integrated light scattering intensities or the invariants for both crossed and parallel geometries, respectively, as

$$Q_\delta = \int_0^\infty I_{Hv} Q^2 \, \mathrm{d}Q \propto \langle \delta^2 \rangle \qquad (5)$$

and

$$Q_\eta = \int_0^\infty \left(I_{Vv} - \left(\frac{4}{3}\right) I_{Hv} \right) Q^2 \, \mathrm{d}Q \propto \langle \eta^2 \rangle \qquad (6)$$

Here $\langle \delta^2 \rangle$ and $\langle \eta^2 \rangle$ are the mean square orientation and density fluctuations, respectively. It should be noted here that the integrated intensities within finite Q ranges were practically employed instead of the invariants. Thus, the integration Q ranges for Q_δ and Q_η are 0.7–2.2 μm^{-1} and 2–6 μm^{-1}, respectively; in other words they are seeing larger and smaller regions in size, respectively. However, for the sake of convenience these symbols will be used thereafter.

The in situ crystallization time dependences of Q_δ and Q_η are shown in Fig. 14. As seen from this figure, the crystallization time dependence of Q_δ shows sigmoidal shape very similar to the crystallization isotherm and begins to increase in 20 s of annealing time, while the Q_η starts to increase immediately after the sample temperature reached 220 °C and has a maximum at crystallization time 350 s.
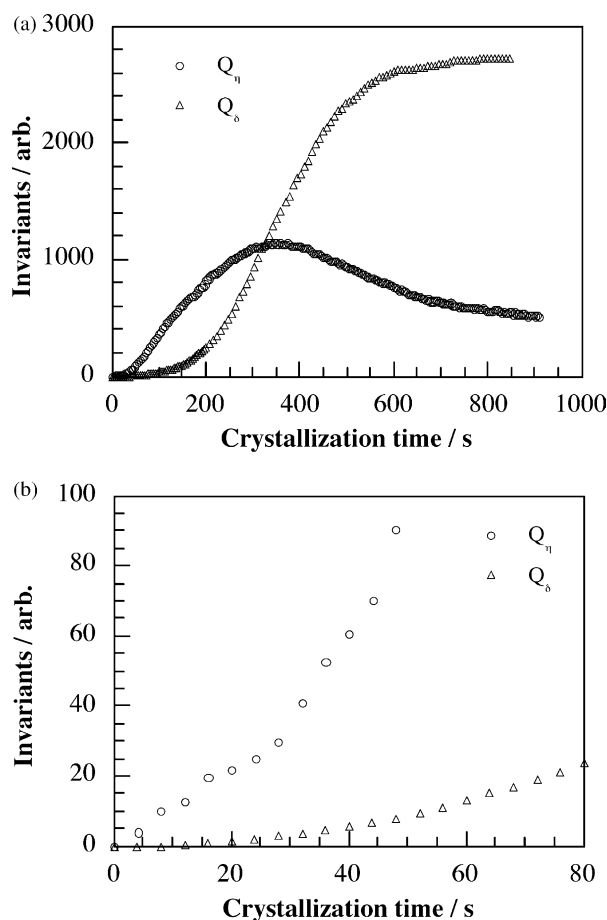

Fig. 12. Plot of $I^{-1/2}$ vs Q^2 for a PET sample annealed for 10 s at 220 °C.

Fig. 14. Crystallization time dependences of the integrated light scattering intensities Q_δ and Q_η during the annealing of the PET sample at 220 °C. (a) 0–900 s, (b) enlargement of (a) in the initial time range of 0–80 s.

Similar behaviours were reported for the early stage of crystallization in isotactic polypropylene as well by Okada et al. [49]. Different views for this similar observations will be discussed later.

3.5. Internal structure of the spherulite

The three experimental results described above suggest that the particle structure of the PET sample is not an artifact on preparing samples but a real one. Below, the relationship between the particle structure and the spherulites has further been studied. Fig. 15 shows an enlarged SEM photograph of the fibrils on the spherulite surface.

A dominant fibril with a diameter of about 1 μm branches at some points to thinner subsidiary fibrils with a diameter about 0.2 μm which grow to another directions. It is presumed as well that the thinner fibrils are formed by the fusion of the small particles with a diameter of about 0.15 μm because the spherical shape is seen in a part of one of the fibrils. Hence, it may be considered that the small particles are structural units. However, it should be noted that the many finest fibrils, which are seen at the bottom of the photograph, are not original structure but artifacts, which were caused when the specimen was stripped off from the surface of a spherulite by peeling.
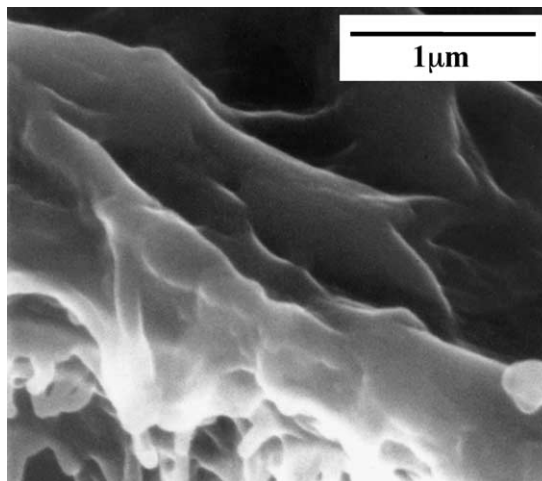

Fig. 15. SEM photograph of fibrils stripped off from the surface of a PET spherulite. Thinnest fibrils below are produced by a drawing effect when the fibrils were stripped off from the spherulite surface.

4. Discussion

Before the discussion, the readers would be reminded of the above important observations and our concept described in Section 1, which was also reviewed in literature [18]. As seen from Fig. 5, the internal structure of the growing spherulite at the initial stage is filled with the small particles. This seems to mean that a spherical entity, named the droplet in this paper, must have been formed prior to the emergence of the small particles inside it. Such a spherical entity or droplet may be considered an optically anisotropic nucleus caused by the N & G type primary phase separation of the melt, which was predicted by Olmsted et al. [19], since the PET melt at 220 °C is in the metastable state judging from our previous observation that the spinodal temperature T_s for PET is 213 °C [30]. As described before, the critical size of the nucleus in the N & G mechanism was estimated from Fig. 10 to be a few micrometer. This N & G process should begin at less than 10 s since the small particles appeared by this time (Fig. 6(b)). The initial internal structure of the droplet may be considered the nematic phase of polymer liquid crystal where the stiff molecular segments orient probably perpendicular to the radius of the droplet. Though the textural structure of nematic liquid crystals inside the droplet is a very important problem to be solved in future for better understanding of the growth mechanism and the internal structure of spherulites, it should be noted at the moment that the nematic phase of polymers contains a large amount of molecular entanglements. So, in the next step the nematic phase separates into smectic phase and amorphous phase by the secondary phase separation of SD type where molecular entanglements are excluded from the smectic phase to the amorphous phase. In the final stage of the secondary phase separation of SD type the SD structure changes to the small particles because of the surface tension. Furthermore, the small particles in turn transform to crystalline lamellae by their fusion, resulting in crystalline spherulites.

On the basis of the above concept we discuss the time-dependence of the integrated intensities of Q_δ and Q_η. As shown in the previous section, the crystallization time dependence of Q_δ shows the sigmoidal shape very similar to the crystallization isotherm; it begins to increase in 20 s of annealing time and levels off at around 600 s, while the Q_η starts to increase immediately after the sample temperature reached 220 °C, and then it decreases after reaching a maximum at around 350 s. These behaviours do not contradict essentially with the observations by Okada et al. [49] though our observed Q range of the Vv scattering, 2–6 μm^{-1}, is considerably higher compared with that of Okada et al., 1–2.4 μm^{-1}. The problem is that the explanations for the time-dependences of Q_δ and Q_η are different. They considered that crystalline spherulites appear directly from the beginning. On the other hand, we assume that the optically anisotropic droplets with the nematic phase are first caused by the primary phase separation of N & G type, inside which the small particles are then produced by the secondary phase separation of SD type, and these small particles in turn transform to crystalline lamellae by their fusion, resulting in crystalline spherulites. Such different views cannot be distinguished only from the light scattering measurements as will be shown in the next paragraph. However, we could actually observe the small particle structure inside the droplet in the initial stage of crystallization. Therefore, the behaviours of the integrated intensities will be elucidated in more detail, following our concept.

In the initial time until 150 s it may be considered that the nucleation of the droplets is predominant since the droplet size hardly increases from 4 μm and the molecular orientation, Q_δ, does not very proceed (Figs. 10 and 14a, respectively). After that, the growing process of the droplets starts; the droplet size increases and the molecular orientation Q_δ rapidly proceeds with time, probably with the formation of the small particles inside the droplet, and finally it levels off by the collision of the droplets. The time dependence of the integrated intensity Q_η due to density fluctuations $\langle \eta^2 \rangle$ may be elucidated from the following equation [48]:

$$\langle \eta^2 \rangle = \phi_d(1 - \phi_d)(\alpha_d - \alpha_m) \tag{7}$$

where ϕ_d is the volume fraction of the droplets, α_d is the average polarizability of the droplet, and α_m is the polarizability of the matrix. The Eq. (7) is valid independent of whether the internal structure of the droplet is nematic, smectic or crystalline as far as the polarizabilities of the droplet and the matrix are different. This equation tells us that when the volume fraction ϕ_d of the droplets in the matrix is 50%, the integrated intensity assumes the maximum. Actually when Q_δ is ca. 50% of the level-off value at around 350 s, Q_η has a maximum.

Based on the above discussion, we visualize a possible mechanism of spherulite formation in the following subsection.

4.1. A tentative model for spherulite formation

First, the polymer melt in the metastable state undergoes the primary phase separation of N & G type where the spherical droplets with the structure of nematic phase as the nuclei are produced. The molecular orientation in these droplets is probably perpendicular to the droplet radius. Then, the secondary phase separation of SD type occurs inside the droplet, resulting in a spinodal structure, which in turn changes to small particles owing to surface tension. These particles have the structure of smectic phase from which a considerable amount of entanglements which had been contained in the nematic phase are excluded; their average size was about 150 nm for PET. After a certain time, these particles grow to the anisotropic crystalline lamellae by their radial and azimuthal fusion because the molecular rigid segments of smectic phase in the small particles are oriented nearly perpendicular to the radius of the droplet as schematically shown in Fig. 16. At this stage a usual SAXS long preiod of
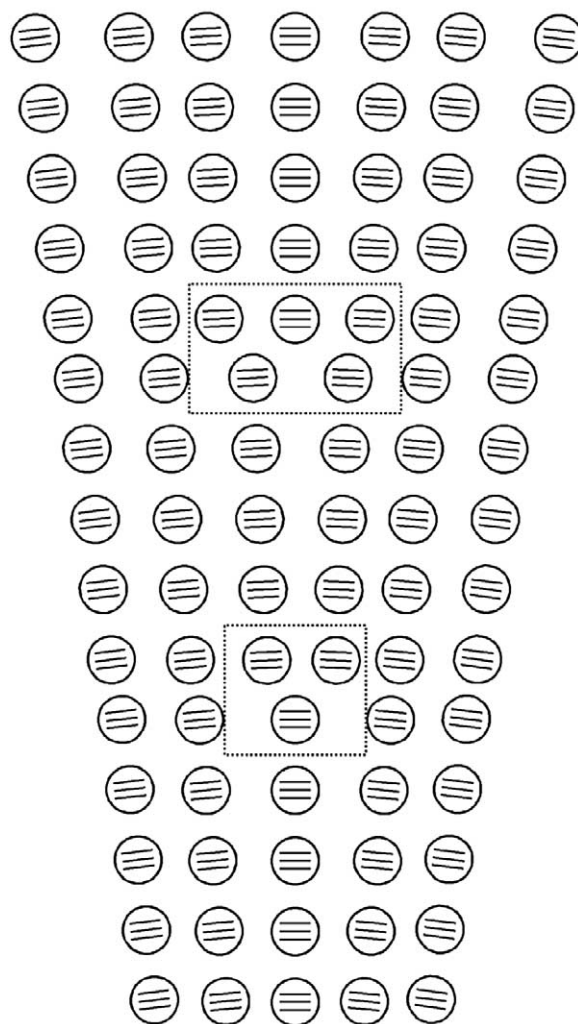

Fig. 16. A schematic model for a part of precursary structure in a spherulite consisting of small particles produced by a secondary phase separation of SD type. The lines in the small particles indicate that the particles have smectic phase where molecular segments orient normal to the radius of the sphere.

about 15 nm for PET appears, but this value is one order of magnitude smaller than the small particle size. This means that the particle fusion provides about 10 layered crystalline lamellae at the same time. Since, the usual long period is due to the alternative structure of the crystal lamella and the amorphous layer, a small amount of entanglements had still remained in the small particles.

Another important point is as follows. In order that the small particles would densely fill the space in the spherical droplet, packing defects as indicated with dotted squares in the figure will be generated inevitably. These defects occurring periodically from the centre of the droplet may provide possible branching points of crystalline fibrils or possible screw dislocation points when crystallization rate is very high; the latter could explain the reason why crystal lamellar screw dislocations appear periodically. At these defect points fused crystalline lamellae change the growing direction slightly with branching. Of course, all the particles are not simultaneously incorporated into the lamellae, and probably the fusion proceeds outwards from the centre since it may be considered that nearer the centre the packing density is higher. The unfused small particles remaining between the first crystallized lamellae, which may be composed of lower molecular weights for an example, would crystallize later also by fusion. The segregation of components with lower molecular weights would occur at the stage of the secondary phase separation of SD type.

References

[1] Hess K. Die Chemie der Zellulose. Leibzig: Akademische Verlagsgesellschaft; 1928.
[2] Bunn CW, Alcock TC. Trans Faraday Soc 1945;41:317.
[3] Keller A. J Polym Sci 1955; 17: 291, 351, 447.
[4] Wunderlich B. Molecular physics. Crystal structure, morphology, defects, vol. I. New York: Academic Press; 1973.
[5] Bassett DC. Principles of polymer morphology. Cambridge: Cambridge University Press; 1981.
[6] Bassett DC. Philos Trans R Soc London A 1994;348:29.
[7] Kaji K. Crystalline and amorphous polymers. In: Gabrys BJ, editor. Applications of neutron scattering to soft condensed matter. Amsterdam: Gordon & Breach; 2000.
[8] Keith HD, Padden FJ. J Appl Phys 1963;34:2409.
[9] White HM, Bassett DC. Polymer 1997;38:5515.
[10] Abo el Maaty MI, Hosier IL, Bassett DC. Macromolecules 1998;31:153.
[11] Bassett DC. Polym J 1999;31:759.
[12] Hosier IL, Bassett DC. Polym J 1999;31:772.
[13] Abo el Maaty MI. Polym J 1999;31:778.
[14] Janimak JJ, Bassett DC. Polymer 1999;40:459.
[15] Bassett DC, Olley RH, Sutton SJ, Vaughan AS. Macromolecules 1996;29: 1852.
[16] Bassett DC, Olley RH, Sutton SJ, Vaughan AS. Polymer 1996;37:4993.
[17] Hosier IL, Bassett DC, Vaughan AS. Macromolecules 2000;33:8781.
[18] Kaji K, Nishida K, Kanaya T, Matsuba G, Konishi T, Imai M. Adv Polym Sci 2005;191:87.
[19] Olmsted PD, Poon WCK, McLeish TCB, Terrill NJ, Ryan AJ. Phys Rev Lett 1998;81:373.
[20] Imai M, Mori K, Mizukami T, Kaji K, Kanaya T. Polymer 1992;33: 4451.
[21] Imai M, Mori K, Mizukami T, Kaji K, Kanaya T. Polymer 1992;33:4457.
[22] Imai M, Kaji K, Kanaya T. Phys Rev Lett 1993;71:4162.
[23] Imai M, Kaji K, Kanaya T. Macromolecules 1994;27:7103.
[24] Imai M, Kaji K, Kanaya T, Sakai Y. Physica B 1995;213/214:718.
[25] Imai M, Kaji K, Kanaya T, Sakai Y. Phys Rev B 1995;52:12696.
[26] Matsuba G, Kaji K, Nishida K, Kanaya T, Imai M. Macromolecules 1999; 32:8932.
[27] Matsuba G, Kaji K, Nishida K, Kanaya T, Imai M. Polymer J 1999;31: 722.
[28] Matsuba G, Kanaya T, Saito M, Kaji K, Nishida K. Phys Rev E 2000;62: R1497.
[29] Matsuba G, Kaji K, Kanaya T, Nishida K. Phys Rev E 2002;65: 061801–0618011.
[30] Nishida K, Kaji K, Kanaya T, Matsuba G, Konishi T. J Polym Sci B; Polym Phys 2004;42:1817.
[31] Nishida K, Konishi T, Kanaya T, Kaji K. Polymer 2004;45:1417.
[32] Kaji K, Nishida K, Matsuba G, Kanaya T, Imai M. J Macromol Sci B 2003;42:709.
[33] Strobl G. Eur Phys J E 2000;3:165.
[34] Ryan AJ, Fairclough JPA, Terrill NJ, Olmsted PD, Poon WCK. Faraday Discuss 1999;112:13.
[35] Heeley EL, Kit Poh C, Li W, Maidens A, Bras W, Dolbnya IP, et al. Faraday Discuss 2002;122:343.
[36] Heeley EL, Maidens AV, Olmsted PD, Bras W, Dolbnya IP, Fairclough JPA, et al. Macromolecules 2003;36:3656.
[37] Wang Z-G, Hsiao BS, Sirota EB, Agarwal P, Srinivas S. Macromolecules 2000;33:978.
[38] Wang Z-G, Hsiao BS, Srinivas S, Brown GM, Tsou AH, Chen SZD, et al. Polymer 2001;42:7561.
[39] Muthukumar M, Welch P. Polymer 2000;41:8833.
[40] Muthukumar M. Philos Trans R Soc London, A 2003;361:539.
[41] Boon J, Challa G, van Krevelen DW. J Polym Sci A-2 1968;6(1791): 1835.
[42] Van Krevelen DW. Properties of polymers. 3rd ed. Amsterdam: Elsevier 1990;585.
[43] Flory PJ. Proc R Soc A 1956;234:60.
[44] Hayashi H, Hamada F, Suehiro S, Masaki N, Ogawa T, Miyaji H. J Appl Cryst 1988;21:330.
[45] Samuels RJ. J Polym Sci A-2 1971;9:2165.
[46] Debye P, Buche AM. J Appl Phys 1949;20:518.
[47] Herglotz HK. J Colloid Interf Sci 1980;75:105.
[48] Koberstein J, Russel TP, Stein RS. J Polym Sci; Polym Phys Ed 1979;17: 1719.
[49] Okada T, Saito H, Inoue T. Macromolecules 1992;25:1908.